Journal of Applied Polymer Science

Carbon nanohorn and graphene nanoplate based polystyrene nanocomposites for superior electromagnetic interference shielding applications

Ranadip Bera, Supratim Suin, Sandip Maiti, Nilesh Kumar Shrivastava, Bhanu Bhusan Khatua
Materials Science Centre, Indian Institute of Technology, Kharagpur 721302, India
Correspondence to: B. B. Khatua (E-mail: khatuabb@matsc.iitkgp.ernet.in)

ABSTRACT: In this article is reported the preparation of carbon nanohorn (CNH)/graphene nanoplates (GNP)/polystyrene (PS) nanocomposites through in-situ bulk polymerization of styrene monomer in the presence of CNH, followed by the addition of suspension polymerized GNP/PS bead during polymerization of styrene, as next-generation multifunctional material for high electrical conductivity and electromagnetic interference shielding effectiveness (EMI SE) applications. Morphological analysis revealed selective dispersion of CNH in bulk polymerized PS matrix, where GNP/PS beads were randomly distributed. The formation of continuous CNH–CNH conductive path and GNP–CNH–GNP or CNH–GNP–CNH conductive network throughout the PS matrix at exceptionally low loading of CNH (1.0 wt %) and GNP (0.15 wt %) leads to high electrical conductivity (6.24×10^{-2} S cm^{-1}) and EMI SE ~(−24.83 dB) when the nanocomposites was prepared in the presence of 75 wt % GNP/PS bead. © 2015 Wiley Periodicals, Inc. J. Appl. Polym. Sci. **2015**, *132*, 42803.

KEYWORDS: molding; morphology; polystyrene

Received 19 May 2015; accepted 1 August 2015
DOI: 10.1002/app.42803

INTRODUCTION

Recently, materials having good electromagnetic interference (EMI) shielding efficiency have attracted great attention in various academic and industrial areas due to rapid increase of electromagnetic pollution produced by various electronics devices. Conventional metal-based EMI shielding materials which own the disadvantages of easy corrosion, heavy weight, physical rigidity, and poor processibility in edges, corners, and tips have very weak wave absorption property. Effective EMI Shielding efficiency through wave absorption, light weight, low cost, and easy processability properties are the main criteria for the next-generation EMI shielding materials and can be fulfilled by nanofillers/polymer-based nanocomposites or conductive polymer nanocomposites. For example, carbon nanomaterials like carbon nanotubes (CNT),[1–6] carbon nanofiber (CNF),[7] and graphene[8,9] are incorporated into the matrix polymer to prepare light-weight efficient EMI shielding materials that can be used not only in defense and space applications but also in commodity electronics. In recent years, researchers are trying to improve the EMI shielding efficiency through developing different types of morphology in polymer nanocomposites using different nanofillers. For example, Kim *et al.*[10] prepared multilayer EMI shielding materials where reduced graphene oxide (RGO) sheets interleaved between polyetherimide (PEI) films fabricated by electrophoretic deposition (EPD) and achieved 6.37 dB EMI SE value at 0.66 vol % of RGO loading. Jiang *et al.*[11] reported that ultrahigh molecular weight polyethylene (UHMWPE)/graphite nanocomposites with a typical segregated structure shows 51.6 dB EMI SE value at 7.05 vol % graphite loading. Tran *et al.*[12] prepared polypropylene/CNT nanocomposites foam which can absorb 90% of microwave in the frequency ranges 25–40 GHz. In our study, a heterogeneous architecture with multiple nanofillers was developed for the polymeric system to enhance the EMI Shielding efficiency.

Through the increasing conductive network and the scattering of microwave in the nanocomposites, we can increase the EMI shielding effectiveness through reflection and absorption of microwave. Among the different nanofillers, single-wall carbon nanohorn (CNH) and graphene nanoplate (GNP) have been chosen in this study to fulfill the criteria of a good EMI shielding material, due to their unique properties such as structural, electrical, and mechanical properties. CNH, belonging to the carbon nanostructured materials family, consisting of flower-like architecture with sp^2-hybridized carbon, has many typical properties such as good electrical property, thermal conductivity, ease of functionalization, and so on.[13] Individual nanohorn has an irregular tube shape, looks like a horn with a variable diameter of 2–5 nm, length of 40–50 nm,[14] and horn tip has an

average angle of ~20°.[15] Due to aggregation, nanohorns form spherical cluster-like dahlia flower with an average diameter of about 80 nm[16] and lead to a very high surface area which in turn facilitates gaseous and liquid molecules for being inserted.[17] CNHs are easily dispersible in polymer matrix.[18] The electronic properties of CNHs were theoretically established and explained by Berber *et al.*[19] and Kolesnikov *et al.*[20] The flower-like structure of CNH facilitates the formation of CNH–CNH conductive network through their multiple contact points and offers high EMI SE value with concomitant increase in electrical conductivity. It is assumed that the structural arrangement of CNH can create many dead arms which appears as micro capacitors and many number of polarization center in the nanocomposites. CNH is paramagnetic in nature and a typical CNH consist of ~10,000 carbon atoms.[21] The plate-like structure of GNP highly conductive and leads in scattering of microwave. On the other hand, polystyrene (PS) and its derivative like high-impact polystyrene (HIPS) or, styrene acrylonitrile (SAN) are the most common commodity polymers widely used in the electronics industry and packaging applications for their properties and easy synthesis process, that influence us to choose it as matrix material in our work. PS, widely used to make electronics cashing, can protect electronics from EMI pollution through making nanocomposites with conductive nanofillers.

This study deals with the preparation of CNH/GNP/PS nanocomposites through in situ bulk polymerization of CNH-dispersed styrene in the presence of suspension-polymerized GNP/PS bead. By optimizing the amount of CNH loading and GNP/PS bead content in the nanocomposite, very high EMI shielding value ~(−24.83 dB) was achieved at an extremely low loading of CNH (1.0 wt %) and GNP (~0.15 wt %). In addition, the nanocomposites show high electrical conductivity (6.24×10^{-2} S cm^{-1}) at 1.0 wt % CNH and 0.15 wt % GNP loadings. The GNP/PS bead acts as an "excluded volume" in the nanocomposites which increases the effective concentration of the CNH in the in situ bulk polymerized PS region and plays an important role to enhance the EMI shielding value of the nanocomposites. Through the multiple contacts, point CNH forms CNH–GNP–CNH network and CNH–CNH conductive path in the presence of GNP/PS bead. The electromagnetic microwaves absorption was enhanced by reflecting and scattering between the bead wall and nanofillers. Our prepared PS-based nanocomposites can replace other materials in various commercial grounds like electronic casing and packaging where PS is widely used, due to its facile preparation method and such high EMI SE value (easily suppress the commercial requirement of EMI SE value −20 dB) at a very low loading of filler.

EXPERIMENTAL

Materials Details

Synthetic-grade styrene monomer used in this study was procured from Merck, Germany. Benzoyl peroxide (BP), used as the polymerization initiator, and polyvinyl alcohol (PVA), used as the suspension stabilizer, were obtained from Merck, India. CNH (purity > 99%, horn diameter 3~5 nm, cluster diameter 60 ~ 120 nm, active surface 250 ~ 300 m^2/g) and graphene nanoplate (GNP) (Multilayer, carbon purity > 99.5%, diameter 5 ~ 25 μm, thickness 8 ~ 10 nm) were procured from J. K. Impex, Mumbai, India. The CNH and GNP were used as received, without any prior chemical modification.

Preparation of Nanocomposites

The purchased styrene monomer was purified before polymerization. For the purification of styrene monomer, aqueous NaOH (5%, 30 mL) solution and styrene monomer (100 mL) were taken separating funnel followed by vigorous shaking for a period of 15 min. After that, it was allowed to stand for 5 min for equilibrium. The monomer was collected from the separating funnel after decanting the aqueous phase. This step was repeated for 6 times followed by washing the styrene monomer with deionized water for five times. Finally, the washed monomer was passed through anhydrous sodium sulphate (Na_2SO_4) and collected as purified monomer.

A suspension polymerization technique was adapted in this study for preparing GNP-loaded PS (GNP/PS) beads, required in the preparation of the final nanocomposites. For the said purpose, calculated amount (0.06 g) of GNP was dispersed in purified styrene monomer (40 mL) through ultrasonication for 2 h at room temperature using a probe-type ultrasonic processor (OSCAR Model: PR-250 probe tip diameter 6 mm, frequency 25 KHz, and ultrasonic power 250 W). Thereafter, in stirring condition, 1.12 g BP was added into the GNP-dispersed styrene monomer and stirred for 30 min. In a three-neck glass reactor, 800 mL water was taken, and fitted with nitrogen (N_2) inlet and refluxing condenser and placed it in an oil bath, positioned on a temperature-controlled magnetic stirrer. Then, 4 g PVA was poured into the water under constant stirring for 45 min. The GNP/styrene/BP mixture was then poured into the reactor under constant stirring (1000 rpm) condition under N_2 atmosphere at 80°C. The reaction was allowed for 8 h under the same reaction condition. Last, after cooling, the GNP-containing PS beads were sieved and washed by methanol. The desired beads were obtained after air drying and subsequent keeping in hot air oven at 50°C for 24 h. From the final weight (~30 g) of the total GNP/PS beads, the GNP content was calculated to be ~0.2 wt %. Here, we have used a fixed GNP content (considerably lower than the P_c value) to create significant mismatch in the dielectric property in the nanocomposites and thus causing high EMI shielding efficiency.

In the next step, the bulk polymerization reaction was carried out in an isolated system, the law of conservation of mass was considered to be maintained, i.e., the final mass of the polymer should be equal to the mass of the monomer initially present in the reactor. Based on this assumption, purified styrene monomer (15 mL) and CNH (0.028 g) were taken and allowed for ultrasonication (2 h) at room temperature to disperse the CNH in the styrene monomer. After complete dispersion, the mixture was transferred into a three-neck reactor, which was connected to N_2 inlet and a refluxing condenser and placed in an oil bath positioned on a temperature-controlled magnetic stirrer. BP (1 wt %), the polymerization initiator, was poured into the CNH/styrene mixture under constant stirring condition and the temperature of the reactor was allowed to gradually increase to

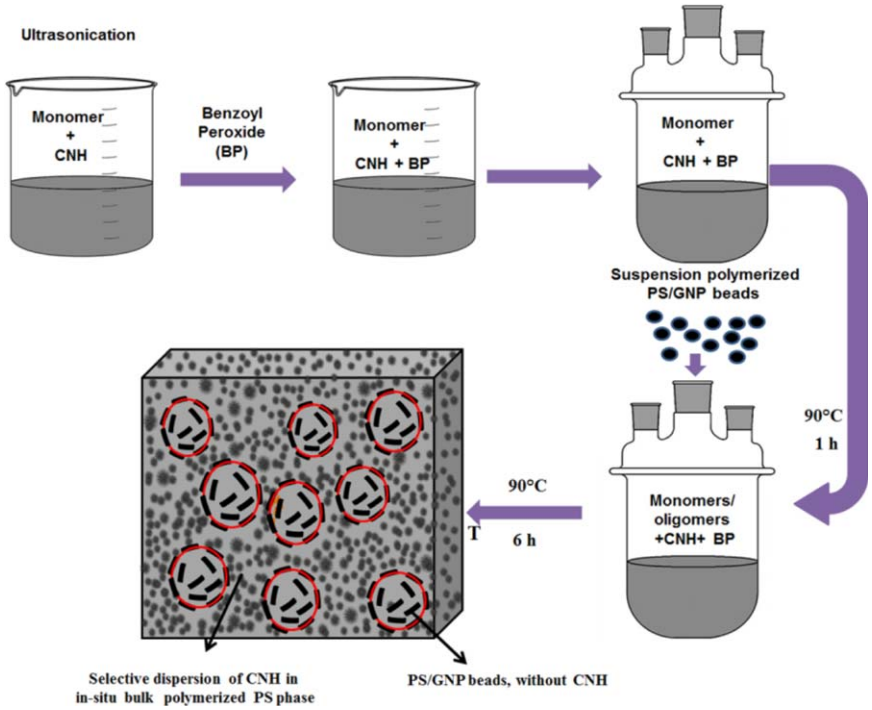

Figure 1. Schematic for the preparation of CNH/GNP/PS nanocomposites. [Color figure can be viewed in the online issue, which is available at wileyonlinelibrary.com.]

~85°C. The GNP/PS beads (15 g) were added into the reaction mixture (after ~1 h) during the polymerization reaction as soon as the reaction mixture became viscous (i.e., in the oligomeric stage). Initially, the swelling of GNP/PS beads occurred in the medium due to co-polymerization, with very nominal migration of CNH onto the bead surface. The reaction was continued for 5 h in N_2 atmosphere at the same reaction condition and the resulting nanocomposites was first air dried for 24 h followed by final drying in a hot air oven at 50°C for 24 h. From the final weight of the prepared nanocomposites (27.27 g), the loading of CNH (~0.10 wt %) and GNP/PS bead (55 wt %) were calculated. Nanocomposites of varying CNH content (0.20, 0.30, 0.50, and 1.0 wt %) were also prepared following the same procedure at the same ratio (45/55 w/w) of (CNH/PS)/(GNP/PS) (loaded with 0.2 wt % GNP). In addition, CNH/GNP/PS nanocomposites with different GNP/PS bead loading (65 and 75 wt %) were prepared at the abovementioned content of CNH (0.10, 0.20, 0.30, 0.50, and 1.0 wt %) following the same polymerization procedure. Finally, the bulk polymerized nanocomposites with various content of CNH, as well as, the GNP/PS bead were compression molded in a hot press under constant pressure (2 MPa) at 160°C. The molded specimens were obtained after cooling. Figure 1 schematically presents the preparation of the nanocomposites.

Characterization

Initially, a high-resolution transmission electron microscope (HRTEM, JEM-2100, JEOL, Japan) was used for morphological investigation of the bulk of the CNH/GNP/PS nanocomposites. The nanocomposites were ultramicrotomed cryogenically with a thickness of 70 ~ 100 nm, and casted on copper grids. All the bright-field images were taken at an accelerating voltage of 200 kV. As the CNH and GNP possess much greater electron density as compared to that of the polymers, no staining was required and the nanofillers appeared as dark in the micrographs.

The field-emission scanning electron microscope (FESEM, Carl Zeiss-SUPRA 40) was used to study the surface morphology of CNH/GNP/PS nanocomposites with an accelerating voltage of 5 kV. The FESEM images were taken on the cryofractured surface of the molded samples after coating with a thin layer of gold to avoid electrical charging. The size of GNP/PS bead was viewed through a scanning electron microscope (SEM, VEGAII LSU, TESCAN, Czech Republic).

A two-probe technique was followed to measure the electrical conductivity of the prepared nanocomposites. The compression molded bars (10 ~ 30 × 10 × 3 mm^3) were used to measure the DC conductivity (σ_{DC}) of the nanocomposites samples. The two ends of the samples bars were cryofractured and the surfaces of the fractured sides were coated by silver paste to ensure good contact between the sample and the electrodes. Equation (1) was used to evaluate the σ_{DC}:

$$\sigma_{DC} = IL/VA \quad (1)$$

Where, I, V, and L represent current, voltage, and length of the samples, respectively. The precise value of σ_{DC} is obtained from the average conductivity value of various lengths of samples.

The compression molded CNH/GNP/PS nanocomposites slabs (25.5 × 13 × 2, 3, 4 mm^3) were used to measure the EMI shielding effectiveness. The measurement was performed by an

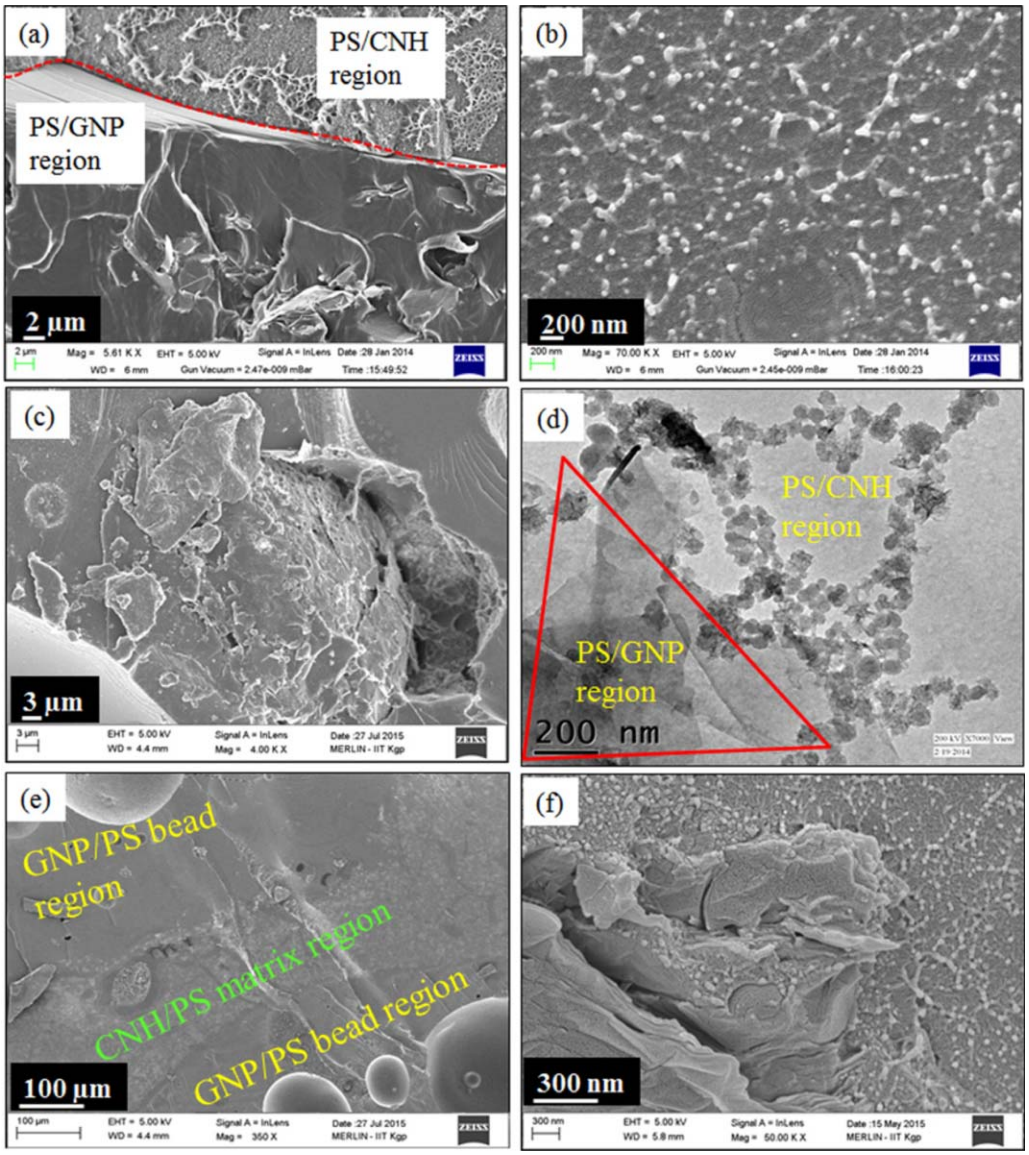

Figure 2. FESEM image of the CNH/GNP/PS nanocomposites displaying (a) GNP/PS bead and CNH/PS junction, (b) CNH/PS bulk polymerized region, and (c) GNP/PS bead region; HRTEM image of CNH/GNP/PS nanocomposites displaying (d) CNH-GNP network. [Color figure can be viewed in the online issue, which is available at wileyonlinelibrary.com.]

E5071C ENA series network analyzer (Agilent Technologies) placing the rectangular specimens between the two port of the waveguide. The S parameters (S_{11}, S_{12}, S_{21}, and S_{22}) of each sample recorded in the X band (8.2–12.4 GHz) frequency range. The total SE, shielding by absorption, and shielding by reflection were calculated from the recorded S parameter of the nanocomposites slab. The complex permittivity and permeability were evaluated from S parameter following a MATLAB code based on Nicolson–Ross–Weir method[22] of the nanocomposites slab.

The thermogravimetric analysis (TGA) of synthesized pure PS and GNP/CNH-containing PS nanocomposites was studied using a TGA V 50 IA Dupont 2100 thermogravimetric analyzer in air atmosphere in the temperature range of 30–600°C with a heating rate of 10°C/min.

RESULTS AND DISCUSSION

Morphology

Figure 2(a) displays the FESEM images of the CNH/GNP/PS nanocomposite. The existence of CNH and GNP which help to make CNH–GNP–CNH conducting network path throughout the nanocomposites is evident from the micrograph. This image also supports the rare penetration of CNH inside the GNP/PS beads and selective dispersion of CNH in the in situ bulk polymerized PS phase. The FESEM image of the CNH/GNP/PS nanocomposites at low magnification [Figure 2(e)] clearly displays the bead and matrix region. The higher magnification FESEM image of bead and matrix interface was shown in Figure 2(f). Figure 2(b) is the higher magnification image of the in situ bulk polymerized PS region of Figure 2(a) in the nanocomposites. This high-magnification image revealed that CNHs were dispersed homogeneously throughout the host polymer. Figure

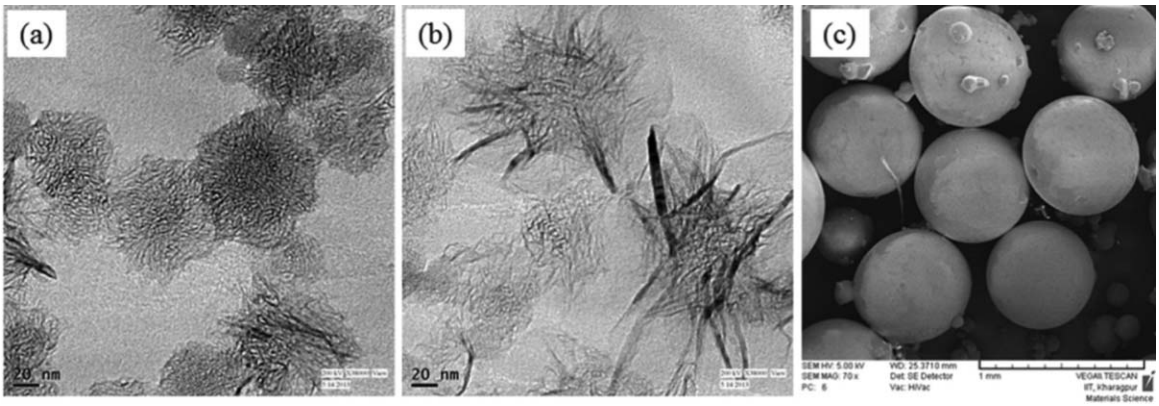

Figure 3. HRTEM images of CNH/GNP/PS nanocomposites displaying (a) CNH-CNH conductive path, (b) flower like structure of CNH, and (c) the SEM image of suspension polymerized GNP/PS bead.

2(c) represents the high-magnification FESEM image of the GNP/PS bead portion, and displays the existence and distribution of GNP in the bead. The HRTEM image [Figure 2(d)] of CNH/GNP/PS nanocomposites supports the presence of CNH and GNP, and confirmed the selective dispersion of CNH in matrix phase, and the formation of CNH–GNP–CNH conducting network structure in the nanocomposites.

Additionally, formation of CNH–CNH conductive path was evident throughout the CNH/PS matrix. CNH has flower-like structure and tends to agglomerate due to van der Walls force of interaction. In this nanocomposite, CNH was allowed to sonicate in the styrene monomer for long time before polymerization. This enables good dispersion of CNH in the monomer. During polymerization process, the viscosity increases which facilitate the secondary agglomeration phenomena of CNH in the nanocomposites.[23] At the time of secondary agglomeration, the flower-like structure of CNH formed CNH–CNH network through its multiple contact points. The contacts between individual CNHs to form the CNH network throughout the bulk polymerized PS phase is presented in Figure 3(a). The highly symmetrical flower-like architecture can be well depicted from the HRTEM image at higher magnification [Figure 3(b)]. The SEM image of suspension-polymerized GNP/PS bead is presented in Figure 3(c). The average diameter of the GNP/PS bead is 600 μm measured by Vega TC software.

Electrical Analysis (DC Conductivity Measurement)

As can be seen, the σ_{DC} value of CNH/GNP/PS nanocomposites was gradually increased with the increase in CNH loading [Figure 4(a)], as well as, the in situ suspension-polymerized GNP/PS bead content [Figure 4(b)]. Thus, an optimum σ_{DC} value (6.24×10^{-2} S cm^{-1}) was evident in the CNH/GNP/PS nanocomposites with 75 wt % GNP/PS bead loading and 1.0 wt % loading of CNH in the bulk polymerized PS phase. It is noteworthy that the CNH/PS nanocomposites with 0.1 wt % CNH show an electrical conductivity $\sim 1.1 \times 10^{-13}$ S cm^{-1}, similar to that of insulating PS. However, the addition of 55 wt % of GNP/PS bead into bulk polymerized PS phase leads to a tremendous improvement in electrical conductivity ($\sim 2.24 \times 10^{-6}$ S cm^{-1}) at the same CNH loading.

Two phenomena might be originated to reveal such high electrical conductivity in the prepared nanocomposites in the presence of GNP/PS beads. First, in the presence of GNP/PS bead, the effective concentration of the CNH greatly increased in the bulk polymerized PS phase of the CNH/GNP/PS nanocomposites and thus, facilitates the formation of CNH–CNH conductive path throughout the PS matrix. As the GNP/PS bead was added at the oligomeric stage of polymerization, the CNH can be assumed to be rarely penetrated in the outer surface of the bead, rather concise in the bulk polymerized region to increase the effective concentration of CNH. Second, in the presence of GNP/PS bead, the conducting nanofillers itself form CNH–GNP–CNH or GNP–CNH–GNP continuous interconnected conducting network at the outer surface of the bead due to surface etching of GNP/PS bead at oligomeric state. So, the incorporation of GNP/PS bead not only increases the effective concentration of CNH in the bulk polymerized PS phase but also takes part in the formation of conductive network due to the presence of conducting GNP in the surface of the suspension-polymerized PS beads.

To explore our considerations, we compare the σ_{DC} value of CNH/GNP/PS nanocomposites containing 0.1 wt % CNH and 75 wt % GNP/PS bead with that of the CNH/PS nanocomposites containing 0.4 wt % of CNH without any bead. As the addition of 75 wt % bead leads to 4 times increment in the effective concentration of CNH, comparable σ_{DC} value is expected for the above considered nanocomposites. Interestingly, the CNH/GNP/PS ternary nanocomposites with 75 wt % GNP/PS bead reveals a superior result as compared to that of the CNH/PS nanocomposites without any bead. This phenomenon unambiguously supports the formation of CNH–GNP–CNH or GNP–CNH–GNP continuous interconnected conducting network in addition to increment in effective concentration of CNH in the prepared nanocomposites, as explained earlier.

Beyond 75 wt % of the GNP/PS bead content, the conductivity of the CNH/GNP/PS nanocomposites starts to fall gradually as the continuity of the CNH–CNH path gets restricted in the presence of bead above an optimum quantity. As the GNPs were preferentially presented on the outer surface of the GNP/PS beads, bulk of the GNP/PS beads was electrically insulating

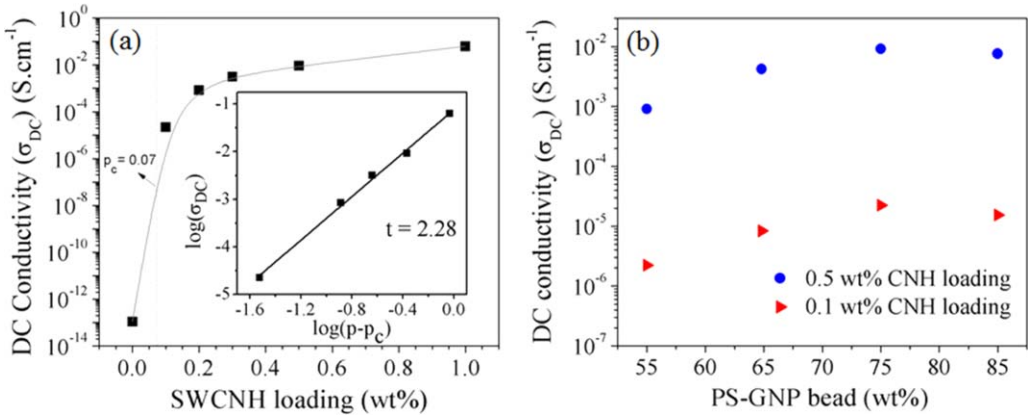

Figure 4. (a) DC conductivity of the CNH/GNP/PS nanocomposites with various CNH loadings at constant weight percent of GNP/PS bead in the PS matrix. The log–log plot of σ_{DC} *versus* $(p - p_c)$ for the nanocomposites was shown in inset of the figure. The straight line in the inset is a least-squares fit to the data using eq. (2), giving the best-fit values $p_c = \sim 0.07$ wt %. (b) DC conductivity of the CNH/GNP/PS nanocomposites with various GNP/PS bead loading. [Color figure can be viewed in the online issue, which is available at wileyonlinelibrary.com.]

in nature. The conductivity value (8.9×10^{-13}) of the GNP/PS bead is almost equal to the conductivity value (1.1×10^{-13}) of PS. Thus, they felt difficulty in the formation of continuous conducting path and resulted in a σ_{DC} value (7.61×10^{-3} S cm^{-1}) for 0.5 wt % CNH containing 85 wt % GNP/PS bead loading, considerably lower than that containing 75 wt % bead.

Several research groups explained the variation of the σ_{DC} value with nanofillers loading in terms of percolation theory.[24,25] The power–law equation (eq. (2)) explains the dependence of the σ_{DC} on the wt % of the conducting filler (p) and percolation threshold concentration (p_c).

$$\sigma_{DC}(p) = \sigma_0(p - p_c)^t \text{ for } p > p_c \quad (2)$$

Here, t stands for the critical exponent. The values of t and p_c for the CNH/GNP/PS nanocomposites can be theoretically calculated from the best-fitted linear plot of log (σ_{DC}) versus log ($p - p_c$) using eq. (2), as shown in the inset of Figure 4(a). Thus, the obtained p_c and t values are ~0.07 wt % and ~2.28, respectively, for the nanocomposites. The t value lower than 2.0 indicates a percolating network involving more number of "dead arms" and it increases with decrease in "dead arms". The t value of ~2.28 for the CNH/GNP/PS nanocomposites indicates the formation of highly network structure of GNP and CNH in the PS matrix. Many researchers[26,27] predicted the t values for two-dimensional (2D) and three-dimensional lattices (3D) from different theoretical calculations. The predicted values for 2D lattice lie between 1.10 and 1.43, and higher than 2.02 for a 3D lattice. Here, the high t is related to the 3D percolating path in our prepared nanocomposites.

Figure 4(a) shows almost constant conductivity beyond 0.3 wt % CNH loading. Conductive nanocomposites system possessing high difference in conductivity between filler and matrix shows similar type of trend of unaltered electrical conductivity beyond a certain loading of conducting filler. In those nanocomposites systems, conductivity saturates at an optimum loading of filler. Beyond this loading, the conductivity of the nanocomposites does not increase, whereas current-carrying capacity of nanocomposites increases. This phenomenon occurs due to fact that the charge carries among the nanofillers not only depend on the physical contact between the nanofillers but also depend on the charge tunneling through the insulating gaps between the conductive nanofillers.

The insulating gaps are created by thin polymer layer between nanofillers. The electron flows from one filler to another through this insulating gap by tunneling and hooping phenomena. This induced a resistance in nanocomposites and limits the conductivity. Many researchers[28] reported the tunneling conduction of electron between CNT–CNT in polymer nanocomposites. The tunneling mechanism is one of the main causes for the variation of the conducting behavior in the polymer nanocomposites. The energy barrier of tunneling depends on the properties of the matrix polymer and also the nanocomposites manufacturing process. Ryvkina *et al.*[29] theoretically define electron tunneling mechanism of conductivity in the polymer/CB nanocomposites. Thus, the electrical conductivity is related by the following equation:

$$\sigma_{DC} \propto \exp(-Ad) \quad (3)$$

Where A stands for the tunnel parameter and d signifies the tunnel distance. Many researchers have already discussed the electrical conductivity in terms of electron tunneling for various conducting polymer nanocomposites. If nanofillers are homogeneously dispersed throughout the insulating matrix polymer, then the average distance (tunnel distance d) between the conducting nanofillers varies with the p value as the given relation:[30]

$$d \propto p^{-1/3} \quad (4)$$

Thus, using the d value (eq. (4)), eq. (3) can be expressed as the following equation:

$$\log(\sigma_{DC}) \propto p^{-1/3} \quad (5)$$

Figure 5 represents the variation of $\log(\sigma_{DC})$ with $p^{-1/3}$ for CNH/GNP/PS nanocomposites. The linear variation (shown in Figure 5) confirms the existence of tunneling mechanism in our prepared nanocomposites. According to Kilbride *et al.*,[31] in polymer nanocomposites, the insulating coating of polymer

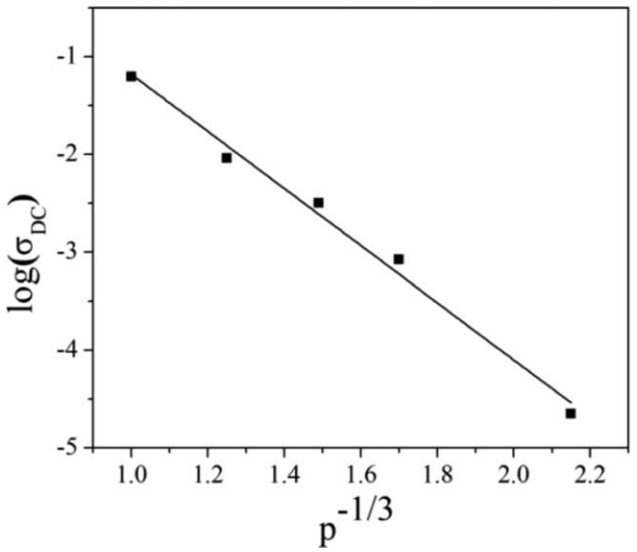

Figure 5. The linear variation of $\log(\sigma_{DC})$ with $p^{-1/3}$ for CNH/GNP/PS nanocomposites.

over nanofillers resists the electrical conductivity due to the enhanced contact resistance among the nanofillers in the presence of polymer.

Thus, the tunneling of electrons through the insulating polymer layer faces difficulty. In fact, the transport of electron from one electrode to another gets restricted due to presence of high-energy insulating polymer layer between them. However, when voltage is applied between the two electrodes, the tunneling of electrons occurs or electron can cross the energy barrier more effectively. CNH has very high surface area and structural defects on its tip can be assumed to favor electron conduction through the electron tunneling mechanism.

Electromagnetic Interference Shielding Effectiveness (EMI SE)

The EMI SE is the ability of a material to control radiated electromagnetic energy. The total EMI shielding performances of a material is considered to be occurred by three mechanisms, viz., reflection, absorption, and internal multiple reflection of radiation. The reflection of radiation occurs by interacting with the free electron or mobile charge carrier (holes) of materials, i.e., reflection occurs due to impedance mismatch. The dielectric constant and the thickness of materials are the determining factors for the absorption or dissipation of electromagnetic radiation in the materials. Multiple reflections are caused by the internal reflection among the internal surfaces of the shielding material, i.e., due to the scattering effect of the in-homogeneity within the materials.[32] This mechanism is typically ignored for single-phase materials.[33] EMI SE (microwave absorption) of materials depends on its DC conductivity, but it is not the only criteria for an efficient EMI shielding material.[34]

The EMI SE value of any material can be calculated using the following equation:

$$\text{EMI SE}_{\text{total}}(dB) = 10\log(P_{in}/P_{out}) \quad (6)$$

Where, P_{in} and P_{out}, respectively, signify the incident and transmitted electromagnetic power. When electromagnetic radiation is incident on the plate of materials, the incident power (P_{in}) of the radiation gets divided into three parts (absorbed power—P_{abs}, reflected power—P_{ref}, transmitted power—P_{out}).

$$P_{abs} = P_{in} - P_{ref} - P_{out} \quad (7)$$

The power co-efficient of reflectivity (R), absorptivity (A), and transmissivity (T) can be expressed in terms of the following relation:

$$A + T + R = 1 \quad (8)$$

The coefficients A, R, and T can be described as $A = P_{abs}/P_{in}$, $R = P_{ref}/P_{in}$, $T = P_{out}/P_{in}$.

The total EMI SE (SE_{total}) value is obtained with the help of the given equation:

$$\text{SE}_{\text{total}} = \text{SE}_A + \text{SE}_R + \text{SE}_M \quad (9)$$

Where SE_A, SE_R, and SE_M are, respectively, the shielding efficiency of materials by absorption, reflection, and multiple internal reflections of electromagnetic radiation. If $\text{SE}_{\text{total}} \geq 15$ dB, the SE_M will be negligible and thus eq. (9) becomes:[35]

$$\text{SE}_{\text{total}} = \text{SE}_A + \text{SE}_R \quad (10)$$

The vector network analyzer attached with either co-axial or quadrilateral wave guide sample holders allows the simultaneous measurements of the reflected and transmitted power at the two ports over a given frequency range. It measures the scattering parameters S_{ij} (phase and magnitude) that are characteristic of the device connected between the two ports: $|S_{11}|^2 = P_{ref}/P_{in}$ corresponds to the power reflected back at port 1, normalized to the incoming source power P_{in}. While $|S_{21}|^2 = P_{out}/P_{in}$ is related to the power transmitted from port 1 to port 2 through the device also normalize the incoming power P_{in}.[36] Thus, the total shielding efficiency (SE_{total}), shielding by reflection (SE_R), shielding by absorption (SE_A), transmitted power (T), and reflected power (R) were calculated based on the S parameter obtained from the vector network analyzer as follows:[34]

$$T = |S_{12}|^2 = |S_{21}|^2 \quad (11)$$

$$R = |S_{11}|^2 = |S_{22}|^2 \quad (12)$$

$$\text{SE}_R = 10\log_{10}(1/1 - |S_{11}|^2) \quad (13)$$

$$\text{SE}_A = 10\log_{10}|1 - |S_{11}|^2/|S_{12}|^2| \quad (14)$$

$$\text{SE}_{\text{total}} = 10\log_{10}1/|S_{12}|^2 = 10\log_{10}1/|S_{21}|^2 \quad (15)$$

As can be seen, the maximum EMI SE value ~(−24.83) dB is evident for the CNH/GNP/PS nanocomposites with 1.0 wt % CNH and 75 wt % GNP/PS bead loading, presented in Figure 6. This value of EMI SE for the nanocomposites in the X-band region was calculated using eq. (15). A minimum EMI SE of ~(−20 dB) is required for the materials to be applicable in the commercial grounds. So, our prepared CNH/GNP/PS nanocomposites (with 1.0 wt % CNH and 75 wt % GNP/PS bead) can easily be used as an efficient EMI shielding material in various commercial and practical purposes. Table I presents the comparative study of our result with other work. The appearance of the high EMI SE value ~(−24.83 dB) in the CNH/GNP/PS nanocomposites at a considerably low loading of CNH can be explained in terms of the presence of the GNP/PS beads in the bulk polymerized CNH/PS matrix.

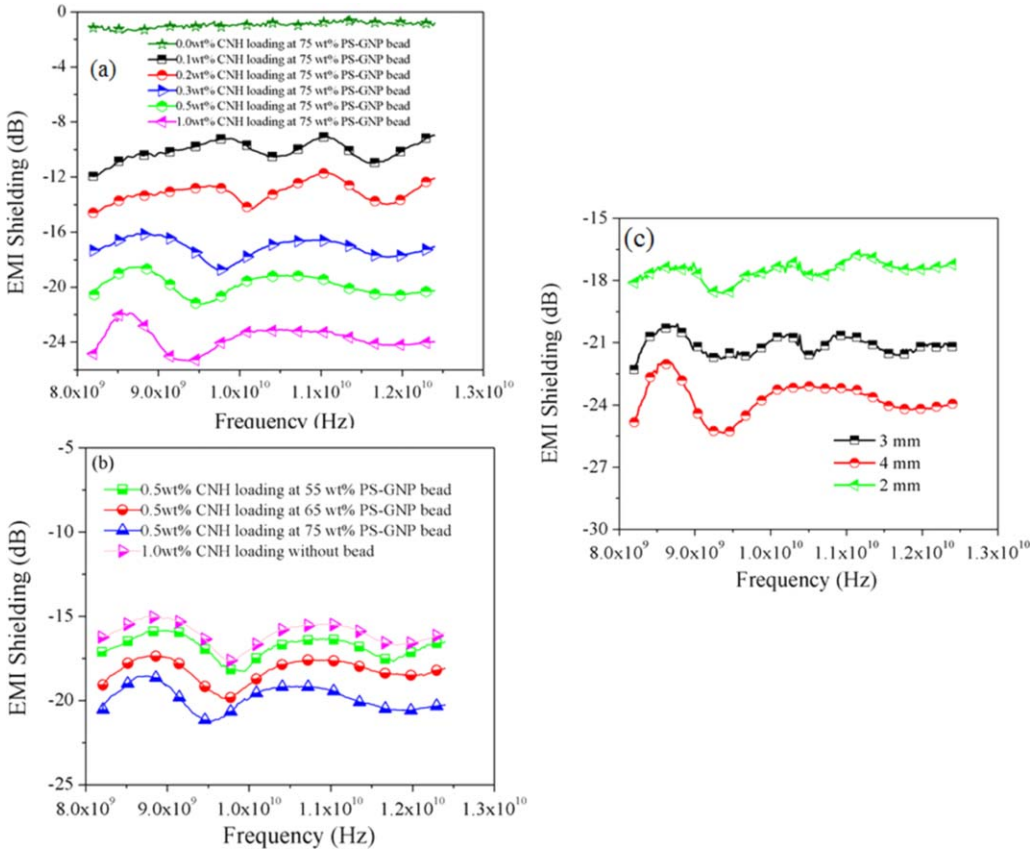

Figure 6. The variation of EMI shielding with frequency of the CNH/GNP/PS (thickness: 4 mm) nanocomposites containing (a) various CNH loadings with constant GNP/PS bead loading (75 wt %), (b) various GNP/PS bead loading at constant CNH loading, and (c) different thickness with 1 wt % CNH and 75 wt % GNP/PS bead loading. [Color figure can be viewed in the online issue, which is available at wileyonlinelibrary.com.]

The incorporated GNP/PS beads act as an "excluded volume" and thus increases the effective concentration of the CNH in the bulk polymerized CNH–PS matrix. As a result, CNH–CNH conductive path forms throughout the matrix phase. Due to the incorporation of GNP/PS bead in the CNH/PS matrix, the concentration of CNH increases around the bead wall [shown in Figure 7(b)]. This phenomenon facilitated in the formation of CNH–GNP–CNH or GNP–CNH–GNP interconnected conductive network at the GNP/PS bead wall by surface etching at oligomeric state, but the inside of the bead remains electrically nonconductive. The microwave reflection occurs due to the impedance mismatch at the interface of the nanocomposite. The microwave absorption property of the nanocomposites related to the conductivity and permittivity of the nanocomposites. The conducting nanofillers (CNH and GNP) interact with the incident radiation of light and play a crucial role to facilitate the electron transport throughout the nanocomposites. The microwave absorption property of the nanocomposites related to the conductivity and permittivity of the nanocomposites. The conducting nanofillers (CNH and GNP) interact with the incident radiation of light and play a crucial role to facilitate the electron transport throughout the nanocomposites. As shown in Figure 7, the presence of nonconductive bead in the nanocomposites could attenuate the incident electromagnetic microwaves by reflecting and scattering between the bead wall and nanofillers, and the microwave were difficult to escape from the sample before being absorbed. The frequency-dependent EMI SE of CNH/GNP/PS nanocomposites with

Table I. Comparison of EMI SE With Other Work

Nanocomposites	Filler loading (wt %)	EMI SE (dB)	Processing method
PS/MWCNT[37]	5	23.50	Dry tumble mixing
PS/PANI/MWCNT[38]	7	−23.30	Solution blending
PS/graphene[39]	30	64.40	Solution mixing
PS/MWCNT[40]	5	15.00	Melt mixing
CNH/GNP/PS (present work)	1.15	−24.83	In-situ polymerization

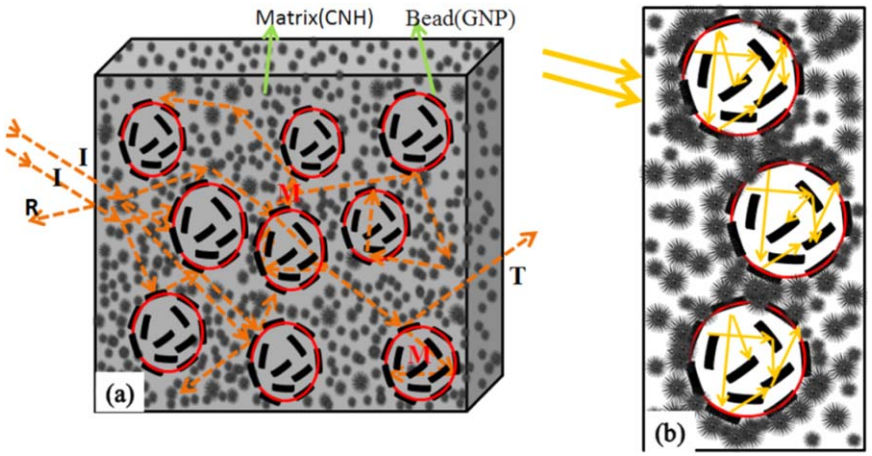

Figure 7. Schematic representation for the effect of GNP/PS bead about the wave scattering, multiple reflections, and the concentration of CNH at the bead wall in the CNH/GNP/PS nanocomposites. [Color figure can be viewed in the online issue, which is available at wileyonlinelibrary.com.]

varying CNH content [Figure 6(a)], as well as, with varying GNP/PS bead content [Figure 6(b)] in the frequency region of 8.2–12.4 GHz (so-called X band region) is shown in Figure 6.

As observed, the EMI SE value increases with increasing the nanofiller (CNH) loading as well as the bead (GNP/PS bead) content in the matrix phase. With the increase of CNH loading, the conductivity value and permittivity value increases which facilitate the microwave absorption as well as EMI SE value. The increase of GNP/PS bead loading in the nanocomposites enhances the microwave absorption through internal multiple reflection.

Moreover, Khatua *et al.*[41] reported that the π–π interaction between the nanofiller and polymer facilitates electron transport in the nanocomposites. In our case, the π–π interaction among the CNH, GNP, and phenyl rings of PS can be operative to improve the EMI SE value of the. Figure 6(b) compares the variation of EMI SE values of CNH/GNP/PS nanocomposites at varying bead content (at fixed 0.5 wt % of CNH) with that of the 1.0 wt % CNH containing CNH/PS nanocomposites prepared without incorporating any bead. As can be seen, the EMI SE values increases with the increase in CNH/PS bead content in the nanocomposites. The effect of GNP/PS bead about the wave scattering and multiple reflections in the CNH/GNP/PS nanocomposites is schematically presented in Figure 7. The microwave absorption property also depends on the thickness of the materials. The shielding effectiveness increases through absorption with the increase of materials' thickness. Figure 6(c) represents the variation of EMI SE of the 1.0 wt % CNH and 75 wt % GNP/PS bead loading CNH/GNP/PS nanocomposites containing various thickness. It shows the EMI SE value increase with the increase of nanocomposites' thickness and the value of EMI SE was maximized at a thickness of 4 mm. Figure 8 illustrates the microwave reflection phenomena in the presence of conductive network structures.

Figure 9 summarizes the contribution of SE_A and SE_R in the total EMI SE value. It can be seen that the SE_A value has the highest contribution in the EMI SE value. Many researchers[42–44] reported the similar value (absorption loss greater than reflection loss) for different types of polymer nanocomposites. The increasing amount of CNH takes part in the formation of more CNH–CNH conductive paths and the CNH–GNP–CNH conductive network which help in microwave absorption through the dissipation of energy. The presence of GNP/PS bead creates difficulty by the CNH–GNP–CNH conductive network for microwave to escape from sample before absorbing. We got maximum of ~81.65% microwave absorption for CNH/GNP/PS nanocomposites at 1.0 wt % CNH and 75 wt % GNP/PS bead loading. The SE_R value also increases with the increase of CNH and GNP/PS bead loading in the nanocomposites. Thus, 18.16% shielding efficiency occurs by reflection for the 1.0 wt % CNH and 75 wt % GNP/PS bead containing CNH/GNP/PS nanocomposites. It is assumed that the CNH–GNP–CNH conductive network also facilitates the microwave reflection in the nanocomposites.

Complex Permittivity and Permeability Analysis

The complex permittivity (ε^*) of the CNH/GNP/PS nanocomposites was evaluated from the S parameter using Nicholson–

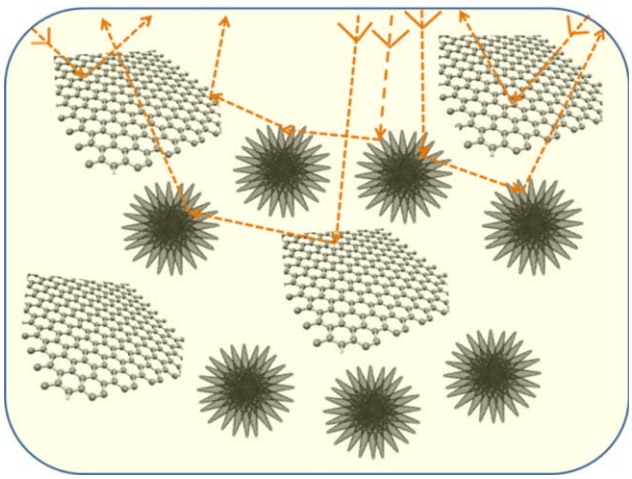

Figure 8. Schematic representation of microwave reflection by CNH–GNP–CNH network. [Color figure can be viewed in the online issue, which is available at wileyonlinelibrary.com.]

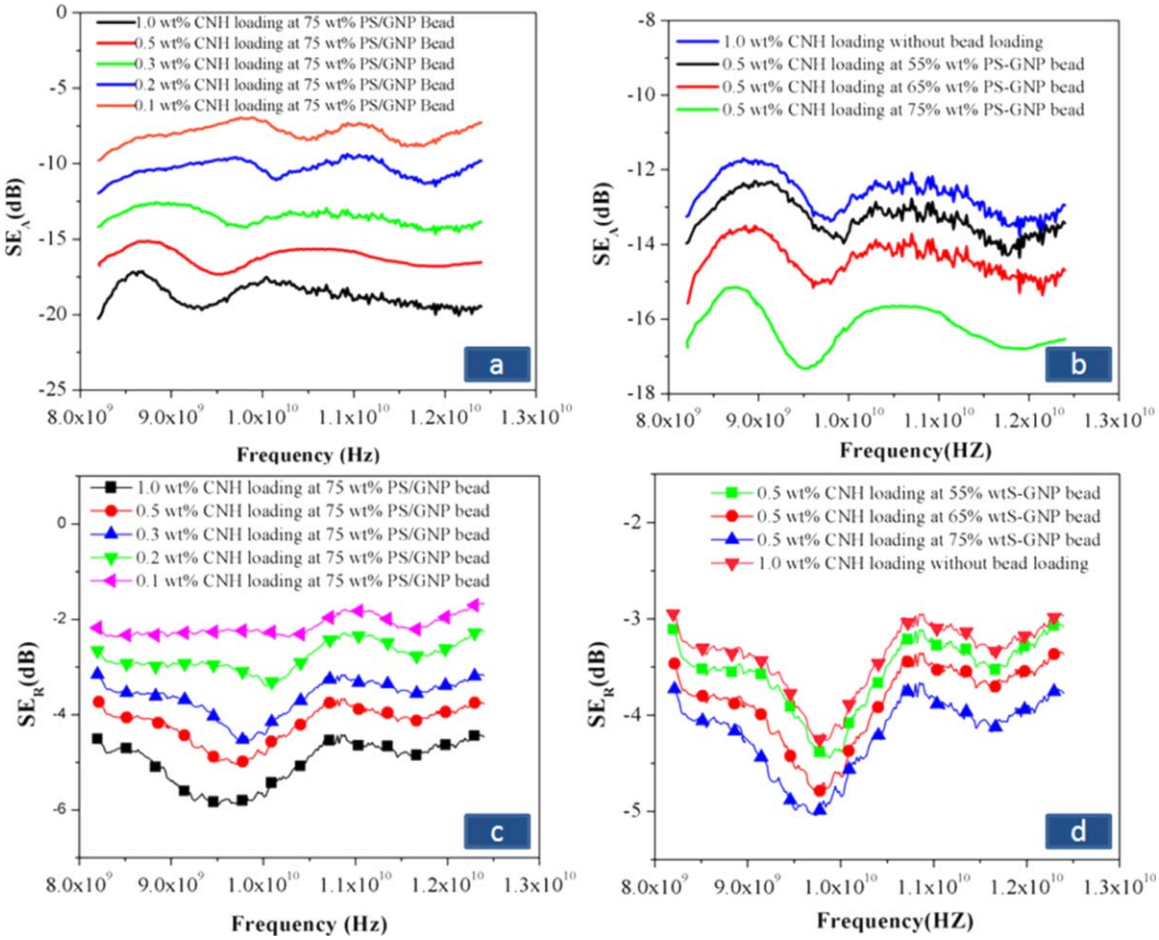

Figure 9. Shielding efficiency by absorption (SE_A) versus frequency at (a) different loading of CNH at constant GNP/PS bead loading, (b) different loading of GNP/PS bead at constant CNH loading, and shielding efficiency by reflection (SE_R) versus frequency at (c) different loading of CNH at constant GNP/PS bead loading and, (d) different loading of GNP/PS bead at constant CNH loading of the CNH/GNP/PS nanocomposites (thickness: 4 mm). [Color figure can be viewed in the online issue, which is available at wileyonlinelibrary.com.]

Ross–Weir method[22] to further investigate the EMI Shielding characteristic. The complex permittivity is represented as

$$\varepsilon^* = \varepsilon' + i\varepsilon'' \tag{16}$$

ε' and ε'' are the real and imaginary components of the complex permittivity, respectively. The real and imaginary components are, respectively, representing the polarization loss and the electric loss. Figure 10 displays the variation of the complex permittivity (real and imaginary) of the CNH/GNP/PS nanocomposites with frequency on varying the loading of CNH at constant GNP/PS bead loading and on varying the GNP/PS bead loading at constant CNH loading.

Figure 10(a,b) clearly revealed that all nanocomposites showed the permittivity (real) increase with the increase of CNH and GNP/PS bead loading. The real permittivity of the nanocomposites is a measure of the number of micro capacitor and polarization centers. The defects in the nanofillers structure create the polarization center.[45] The charge density between polymers matrix and nanofillers aggregation leads to the formation of micro capacitor in the nanocomposites. It is assumed that CNH, due to its flower like structure and tendency of aggregation, can result in many dead arms which appears as micro capacitors and many number of polarization center in the nanocomposites. Thus, the increase of real permittivity occurs with the increase of CNH loading. Furthermore, with the increase of GNP/PS bead loading at constant CNH loading, the real permittivity increases due to the nonconducting nature of the GNP containing PS beads. The presence of GNP creates micro capacitor in the nanocomposites. Moreover, with the increase of CNH loading and GNP/PS bead loading, the gap between the CNH decreases, which increases the polarization of the polymeric materials and consequently enhances the shielding efficiency by absorption.

Figure 10(c,d) represents that the imaginary permittivity, presenting the electric loss, increases with the increases of CNH and GNP/PS bead loadings. In nanocomposites, the mobile charge carriers dissipating through conductive path and network created by the nanofillers. With the increases of CNH and GNP/PS bead loading, the number of conductive path and network increases which leads to higher imaginary permittivity and subsequently higher electromagnetic radiation dissipation by absorption.

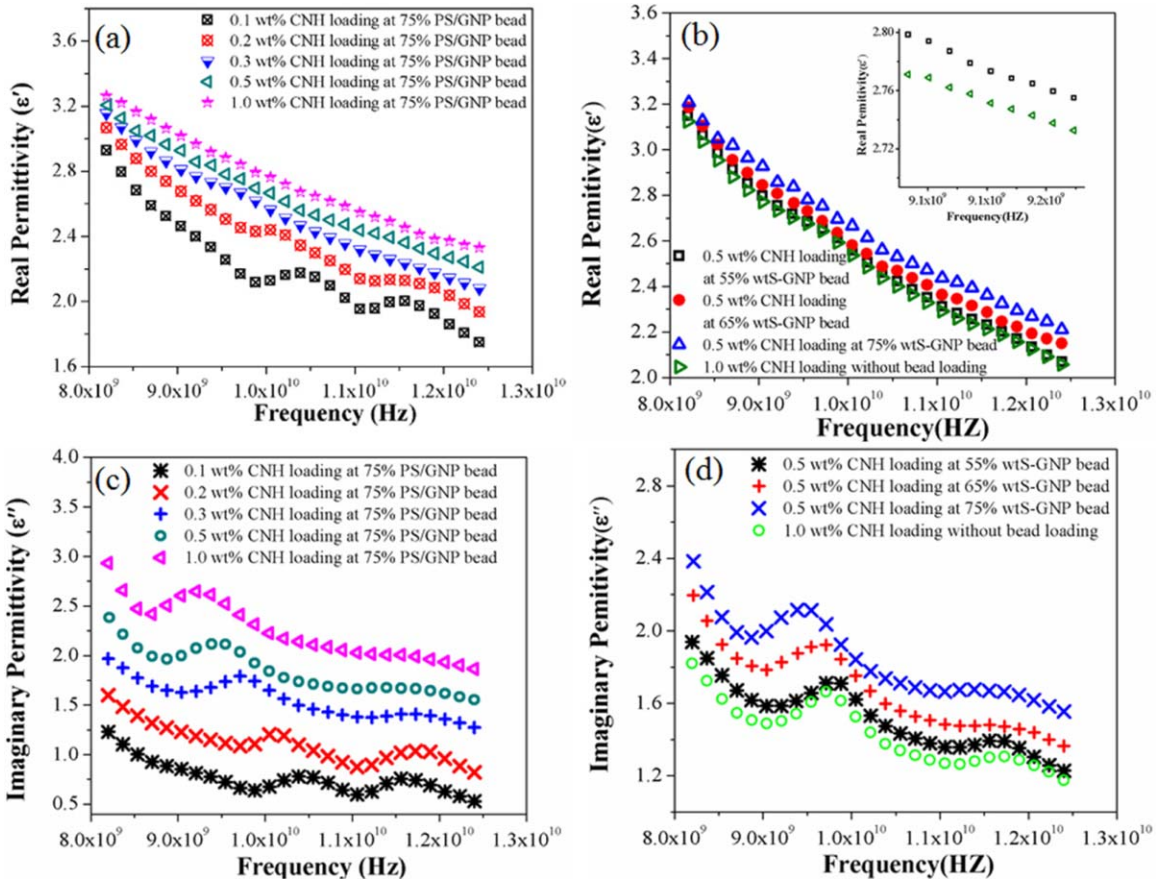

Figure 10. Real permittivity versus frequency at (a) different CNH loading with constant GNP/PS bead, (b) different loading of GNP/PS bead with constant CNH loading and imaginary permittivity versus frequency at (c) different loading of CNH containing constant GNP/PS bead, and (d) different GNP/PS bead loading with constant CNH loading of the CNH/GNP/PS. [Color figure can be viewed in the online issue, which is available at wileyonlinelibrary.com.]

From the *S* parameter, the complex permeability (real and imaginary) of the CNH/GNP/PS nanocomposites was extracted by Nicholson–Ross–Weir method.[22] Figure 11 displays that both the real (μ′) and imaginary (μ″) part are decreases with increase in frequency. The real parts and imaginary parts of complex permeability correlate to the energy storage and loss of electromagnetic wave in materials.[46] The real part of the permeability decreases with the increase of CNH, as well as, GNP/PS bead loading.

The imaginary part of the permeability increases with the increase of CNH and GNP/PS bead loading. The positive imaginary permeability value indicates that the incident electromagnetic energy absorbed by the absorber and the negative imaginary permeability is considered as the electromagnetic energy going out from the absorber.[47] Thus, the increase of imaginary value indicates an increase of microwave absorption with increase in CNH and GNP/PS bead loading.

AC Conductivity

The variation of AC conductivity with frequency at different CNH and GNP/PS bead loading was shown in Figure 12. From the imaginary part of permittivity (ε''), frequency (f), and permittivity of free space (ε_0), the AC conductivity (σ_{AC}) of the nanocomposites can be calculated as follows:[48]

$$\sigma_{AC}(\mathrm{s}\cdot\mathrm{cm}^{-1}) = 2\pi\varepsilon_0\varepsilon'' \quad (17)$$

Similar to σ_{DC}, the σ_{AC} value also increases [Figure 12(a,b)] with the increase of CNH and GNP/PS bead loading in the nanocomposites. This phenomenon supports the concept of the formation and increase of CNH–CNH conducting path and GNP–CNH–GNP conductive network throughout the nanocomposites with the increase of CNH and GNP/PS bead loading. The σ_{AC} value of the nanocomposites remains almost constant in the X-band frequency region, shown in Figure 12(a,b). Based on this observation, we have found a relation between σ_{DC} and σ_{AC}. In this frequency range, the σ_{AC} of samples is remarkably higher than the DC conductivity. It is the evident of the contribution of tunneling and hopping in AC conductivity of the nanocomposites.

TGA Analysis

The TGA of PS and its nanocomposites was represented in Figure 13, and the data obtained are summarized in Table II. The initial degradation temperature (T_0, when materials lost its 10% of total weight) of all the nanocomposites shifted to higher temperature region as compared to synthesized pure PS. Due to low molecular weight and broad molecular weight distribution, pure PS shows less thermal stability. 0.2 wt % GNP-loaded PS nanocomposites show higher thermal stability compared to

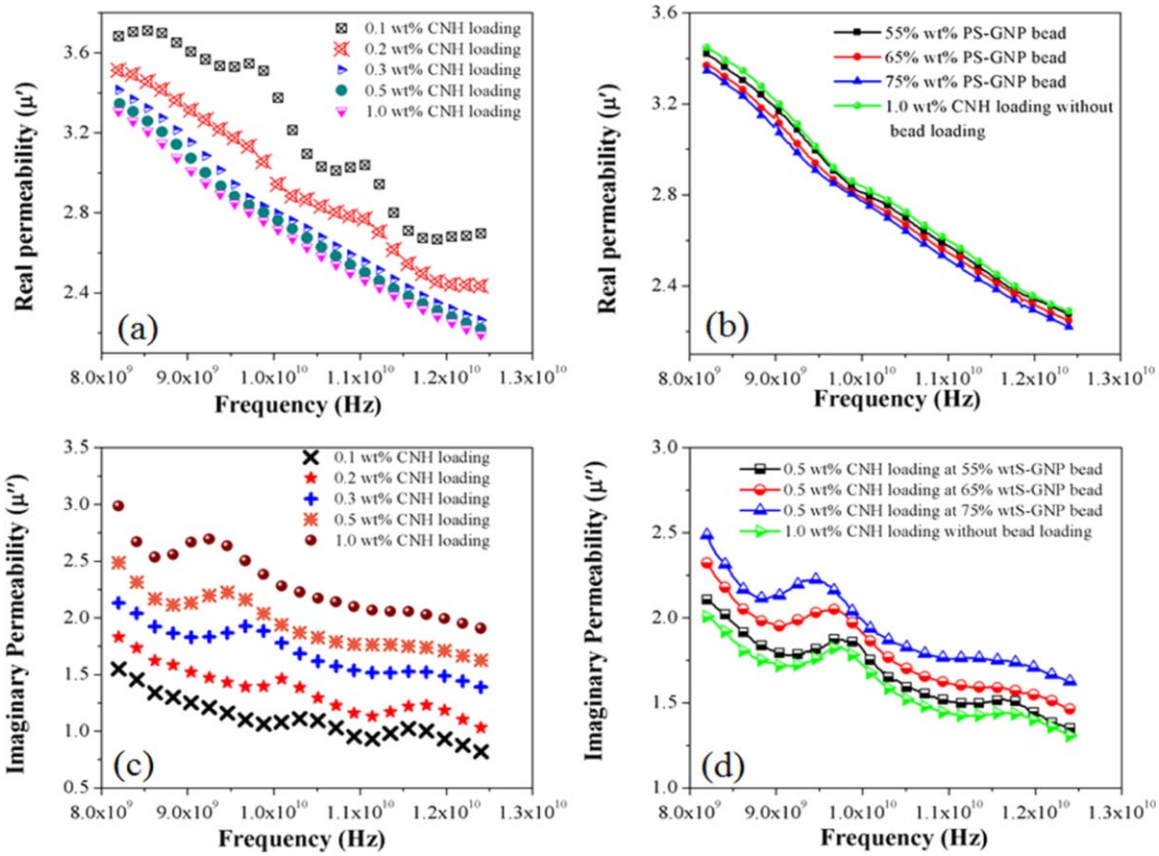

Figure 11. Real permeability versus frequency at (a) different CNH loading with 75 wt % GNP/PS bead loading, (b) different loading of GNP/PS bead containing 1.0 wt % CNH and imaginary permeability versus frequency at (c) different CNH loading with 75 wt % GNP/PS bead, and (d) different GNP/PS bead loading at constant CNH loading of the nanocomposites. [Color figure can be viewed in the online issue, which is available at wileyonlinelibrary.com.]

pure PS. The T_0 value of GNP/PS nanocomposites was slightly increased (from ~287 to 293°C) compared to pure PS, as shown in Figure 13. The maximum initially degradation temperature (T_0 ~ 312°C) was observed for the CNH/GNP/PS nanocomposites containing 1.0 wt % CNH and 75 wt % PS bead (containing 0.2 wt % GNP in the bead). It can be assumed that due to the barrier effect of the dispersed GNP and CNH, the degradation of the polymer was hindered, leading to an increase in initial degradation temperature (T_0) of the nanocomposites. Additionally, the enhanced thermal stability can be

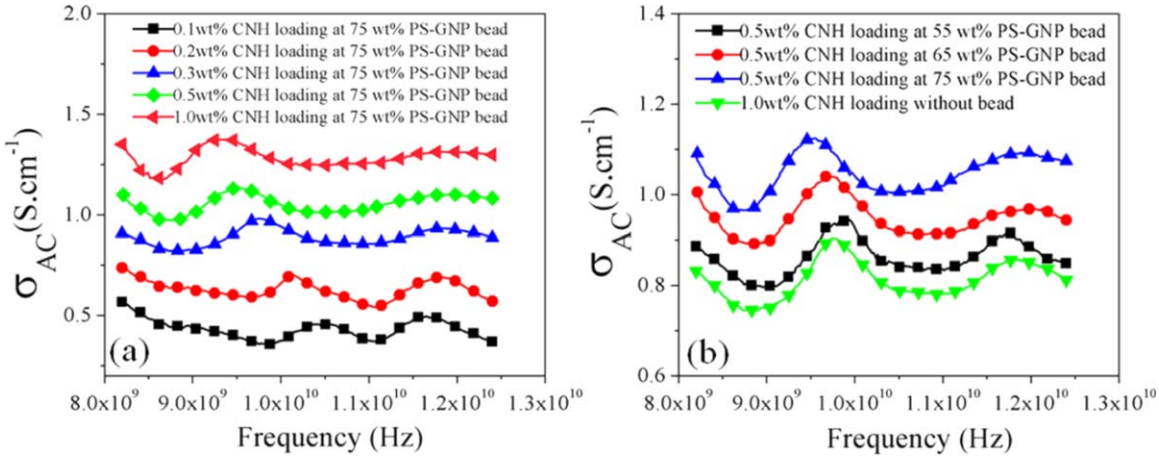

Figure 12. (a) AC conductivity of the CNH/GNP/PS nanocomposites with various CNH loading. (b) The variation of AC conductivity with various GNP/PS bead loading in the CNH/GNP/PS nanocomposites. [Color figure can be viewed in the online issue, which is available at wileyonlinelibrary.com.]

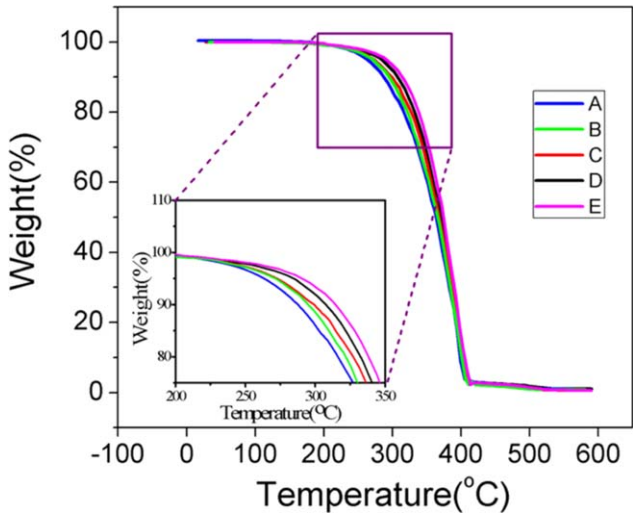

Figure 13. TGA scans of (A) PS and its nanocomposites containing (B) 0.2 wt % GNP, (C) 0.1 wt % CNH and 75 wt % PS bead (with 0.2 wt % GNP in the bead), (D) 1.0 wt % CNH, (E) 1.0 wt % CNH and 75 wt % PS bead (with 0.2 wt % GNP in the bead). [Color figure can be viewed in the online issue, which is available at wileyonlinelibrary.com.]

explained in terms of the strong physical interactions between the adsorbed polymer molecules with the nanofiller surface that delayed the volatilization of polymer.[49]

CONCLUSION

CNH/GNP/PS nanocomposites with high EMI SE value were prepared through a simple method involving the incorporation of suspension-polymerized GNP/PS bead in the in situ polymerized CNH/PS matrix during the polymerization reaction. A considerably high value ~(−24.83 dB) of EMI SE was evident in the nanocomposites with 1 wt % CNH and 0.15 wt % GNP. In addition, the percolation threshold was significantly reduced to 0.07 wt % of CNH in the prepared nanocomposites. The preparatory method involving the addition of GNP/PS beads in situ polymerized PS in the presence of CNH was assumed to be responsible for the high value of EMI SE and the low percolation threshold. The addition of the beads not only acted as excluded volume but also facilitated the formation of GNP–CNH–GNP or CNH–GNP–CNH network structure. However, the contribution from flowerlike geometry of CNH, having high aspect ratio cannot be discarded. The dielectric permittivity (real and imaginary) of the nanocomposites were increased with increase in CNH, as well as, bead loading, i.e., with increase in effective concentration of conductive nanofillers. This method of nanocomposites preparation may open up a new era for developing next-generation multifunctional materials.

Table II. 10 wt % and 50 wt % Degradation Temperature of PS, GNP/PS, and CNH/GNP/PS Nanocomposites

Samples	T_0 (°C)	T_{50} (°C)
A	287	363
B	293	366
C	298	368
D	307	371
E	312	373

We thank the University Grant Commission (UGC), India for their financial support.

REFERENCES

1. Thomason, J. M.; Vulug, D.; Alexandre, M.; Jerome, C.; Molenberg, I.; Huynen, I.; Detrembleur, C. *Polymer* **2012**, *53*, 169.
2. Liu, Z.; Bai, G.; Huang, Y.; Ma, Y.; Du, F.; Li, F.; Guo, T.; Chen, Y. *Carbon* **2007**, *45*, 821.
3. Yang, Y.; Gupta, M. C. *Nano Lett.* **2005**, *5*, 2131.
4. Huang, Y.; Li, N.; Ma, Y.; Du, F.; Li, F.; He, X.; Lin, X.; Gao, H.; Chen, Y. *Carbon* **2007**, *45*, 1614.
5. Joo, J.; Kim, H. M.; Kim, K.; Lee, C. Y.; Cho, S. J.; Yoon, H. S.; Pejakovic, D. A.; Yoo, J. W.; Epstein, A. J. *Appl. Phys. Lett.* **2004**, *84*, 589.
6. Maiti, S.; Suin, S.; Shrivastava, N. K.; Khatua, B. B. *RSC Adv.* **2014**, *4*, 7979.
7. Gupta, M. C.; Yang, Y.; Dudley, K. L.; Lawrence, R. W. *Adv. Mater.* **2005**, *17*, 1999.
8. Yan, D. X.; Ren, P. G.; Pang, H.; Fu, Q.; Yang, M. B.; Li, Z. M. *J. Mater. Chem.* **2012**, *22*, 18772.
9. Yan, D. X.; Pang, H.; Li, B.; Vajtai, R.; Xu, L.; Ren, P. G.; Wang, J. H.; Li, Z. M. *Adv. Funct. Mater.* **2015**, *25*, 559.
10. Kim, S.; Suk Oh, J.; Kim, M.-Gi.; Jang, W.; Wang, M.; Kim, Y.; Seo, Hee Won.; Kim, Y. C.; Lee, J.-H.; Lee, Y.; Nam, J. D. *ACS Appl. Mater. Interfaces* **2014**, *6*, 17647.
11. Jiang, X.; Yan, D.-X.; Bao, Y.; Pang, H.; Ji, Xu.; Li, Z.-M. *RSC Adv.* **2015**, *5*, 22587.
12. Tran, M.-P.; Thomassin, J.-M.; Alexandre, M.; Jerome, C.; Huynen, I.; Detrembleur, C. *Macromol. Chem. Phys.* **2015**, *216*, 1302.
13. Comisso, N.; Berlouis, L. E. A.; Morrow, J.; Pagura, C. *Int. J. Hydrogen Energy* **2010**, *35*, 9070.
14. Zhu, S.; Xu, G. *Nanoscale* **2010**, *2*, 2538.
15. Garaj, S.; Thien-Nga, L.; Gaal, R.; Forro, L.; Takahashi, K.; Kokai, F.; Yudasaka, M.; Iijima, S. *Phys. Rev. B* **2000**, *62*, 17115.
16. Urita, K.; Seki, S.; Utsumi, S.; Noguchi, D.; Kanoh, H.; Tanaka, H.; Hattori, Y.; Ochiai, Y.; Aoki, N.; Yudasaka, M.; Iijima, S.; Kaneko, K. *Nano Lett.* **2006**, *6*, 1325.
17. Fukunaga, Y.; Harada, M.; Bandow, S.; Iijima, S. *Appl. Phys. A* **2009**, *94*, 5.
18. Misra, R. D. K.; Chaudhari, P. M. *J. Biomed. Mater. Res. Part A* **2013**, *101*, 1059.
19. Berber, S.; Kwon, Y. K.; Tomanek, D. *Phys. Rev. B* **2000**, *62*, R2291.
20. Kolesnikov, D. V.; Osipov, V. A. *JETP Lett.* **2004**, *79*, 532.
21. Bandow, S.; Kokai, F.; Takahashi, K.; Yudasaka, M.; Iijima, S. *Appl. Phys. A* **2001**, *73*, 281.

22. Nicolson, A. M.; Ross., G. F. *IEEE Trans. Instr. Measur.* **1970**, *19*, 377.
23. Szczypta, A. F.; Blazewicz, S. *J. Mater. Sci.* **2011**, *46*, 5680.
24. Kirkpatrick, S. *Rev. Mod. Phys.* **1973**, *45*, 574.
25. Stauffer, D.; Aharony, A. Introduction to Percolation Theory, *London: Taylor and Francis*, 2nd ed; **1992**.
26. Fisch, R.; Harris, A. B. *Phys. Rev. B* **1978**, *18*, 416.
27. Gingold, D. B.; Lobb, C. J. *Phys. Rev. B* **1990**, *42*, 8220.
28. Shrivastava, N. K.; Khatua, B. B. *Carbon* **2011**, *49*, 4571.
29. Ryvkina, N.; Tchmutin, I.; Vilcakova, J.; Peliskova, M.; Saha, P. *Synth. Met.* **2005**, *148*, 141.
30. Moniruzzaman, M.; Winey, K. I. *Macromolecules* **2006**, *39*, 5194.
31. Kilbride, B. E.; Coleman, J. N.; Fraysse, J.; Fournet, P.; Cadek, M.; Drury, A.; Hutzler, S.; Roth, S.; Blau, W. J. *J. App. Phys.* **2002**, *92*, 4024.
32. Ling, J.; Zhai, W.; Feng, W.; Shen, B.; Zhang, J.; Zheng, W. G. *ACS Appl. Mater. Interfaces* **2013**, *5*, 2677.
33. Chung, D. D. L. *J. Mater. Eng. Per.* **2000**, *9*, 350.
34. Al-Saleh, M. H.; Saadeh, W. H.; Sundararaj, U. *Carbon* **2013**, 146.
35. Ning, L.; Huang, Y.; Feng, D.; Xiaobo, H.; Xiao, L.; Hongjun, G.; Yanfeng, M.; Li, F.; Chen, Y.; Eklund, P. C. *Nano Lett.* **2006**, *6*, 1141.
36. Thomassin, J. M.; Jerome, C.; Pardoen, T.; Bailly, C.; Huynen, I.; Detrembleur, C. *Mater. Sci. Eng. R* **2013**, *74*, 211.
37. Sachdev, V. K.; Bhattacharya, S.; Patel, K.; Sharma, S. K.; Mehra, N. C.; Tandon, R. P. *J. Appl. Polym. Sci.* **2014**, *131*, 40201.
38. Saini, P.; Choudhary, V. *J. Nanopart. Res.* **2013**, *15*, 1415.
39. Yan, D. X.; Ren, P. G.; Pang, H.; Fu, Q.; Yanga, M. B.; Li, Z. M. *J. Mater. Chem.* **2012**, *22*, 18772.
40. Arjmanda, M.; Apperley, T.; Okoniewski, M.; Sundararaj, U. *Carbon* **2012**, *50*, 5126.
41. Maiti, S.; Shrivastava, N. K.; Suin, S.; Khatua, B. B. *ACS Appl. Mater. Interfaces* **2013**, *5*, 4712.
42. Yuan, B.; Yu, L.; Sheng, L.; An, K.; Zhao, X. *J. Phys. D Appl. Phys.* **2012**, *45*, 235108.
43. Gupta, A.; Choudhary, V. *Compos. Sci. Tech.* **2011**, *71*, 1563.
44. Kim, Y.-Y.; Yun, J.; Kim, H.-I.; Lee, Y.-S. *J. Ind. Eng. Chem.* **2012**, *18*, 392.
45. Watts, P. C. P.; Hsu, W.-K.; Barnes, A.; Chambers, B. *Adv. Mater.* **2003**, *15*, 600.
46. Zhang, X. F.; Huang, H.; Dong, X. L. *J. Phys. Chem. C* **2013**, *117*, 8563.
47. Wang, J. C.; Han, X.; Zhang, X.; Hu, S.; Zhang, T.; Wang, J.; Du, Y.; Wang, X.; Xu, P. *J. Phys. Chem. C* **2010**, *114*, 14826.
48. Reshi, H. A.; Singh, A. P.; Pillai, S.; Yadav, R. S.; Dhawanb, S. K; Shelke, V. *J. Mater. Chem. C* **2015**, *3*, 820.
49. Jin, Z.; Pramoda, K. P.; Xu, G.; S.; Goh, H.; *Chem. Phys. Lett.* **2001**, *337*, 43.